Contract No:

This document was prepared in conjunction with work accomplished under Contract No. DE-AC09-08SR22470 with the U.S. Department of Energy (DOE) Office of Environmental Management (EM).

Disclaimer:

We put science to work.™

Savannah River National Laboratory®

OPERATED BY SAVANNAH RIVER NUCLEAR SOLUTIONS

A U.S. DEPARTMENT OF ENERGY NATIONAL LABORATORY • SAVANNAH RIVER SITE • AIKEN, SC

Interim Report: Blast furnace slag reactions in various solutions

Toward the Development of Designer Slag for LAW Operations

Cory L. Trivelpiece
Madison Hsieh

March 2021

SRNL-STI-2021-00097

SRNL.DOE.GOV

DISCLAIMER

Printed in the United States of America

Prepared for
U.S. Department of Energy

SRNL-STI-2021-00097
Revision 0

Keywords: *blast furnace slag, dissolution*

Retention: *Permanent*

Interim Report: Blast furnace slag reactions in various solutions

Cory L. Trivelpiece
Madison C. Hsieh

March 31, 2021

Prepared for the U.S. Department of Energy under contract number DE-AC09-08SR22470.

REVIEWS AND APPROVALS

AUTHORS:

_____
Cory L. Trivelpiece, Energy Materials Date

TECHNICAL REVIEW:

_____
Christine A. Langton, Materials Science Date

APPROVAL:

_____
Brenda Garcia Diaz, Manager, Energy Materials Date

_____
Joseph Manna, Director, Materials Science Date

PREFACE OR ACKNOWLEDGEMENTS

The research documented in this report was funded by the Department of Energy – Environmental Management Technology Development Office.

EXECUTIVE SUMMARY

Blast furnace slag (BFS) is a critical component of grout formulations for the remediation of low activity nuclear waste. This interim report describes the initial results of a study designed to investigate the fundamental mechanisms of BFS dissolution. The goal of the work is to delineate the physicochemical aspects of the slag that impart beneficial properties to grout formulations to enable the consistent production of a slag-replacement material ("designer slag") that performs better than what is commercially available.

This report documents the dissolution experiments that were conducted using nine different initial solution compositions. Solution measurements for each solution, including pH and solution composition, are given for 1, 7, 14, 28, and 56 day intervals samples. Scanning electron microscopy images are presented for the 56 day samples from each of the solutions. Inferences about reaction mechanisms and 56-day mineralogy are made based on the information collected to date. Some conclusions are made based on the work performed for this interim report, and a path forward including the strategy for making stronger conclusions based on X-ray diffraction (XRD) analyses is presented.

TABLE OF CONTENTS

LIST OF TABLES

LIST OF FIGURES

LIST OF ABBREVIATIONS

BFS	Blast Furnace Slag
C-(N)-A-S-H	Calcium Sodium Aluminosilicate Hydrate
$Ca^{sat.}$	Calcium Saturated
C-S-H	Calcium Silicate Hydrate
DI	De-ionized
ICP	Inductively Coupled Plasma
Ig	Loss-on-ignition
OPC	Ordinary Portland Cement
PCT	Product Consistency Test
RSD	Relative Standard Deviation
SEM	Scanning Electron Microscope
SRNL	Savannah River National Laboratory
SRS	Savannah River Site
XRD	X-ray Diffraction
XRF	X-ray Fluorescence

1.0 Introduction

The use of blast furnace slag (BFS) as an additive material in concrete formulations is a standard practice for many cementitious material applications. This slag, a byproduct of steel production, is a pozzolanic material when ground into a fine powder similar in size distribution to that of ordinary Portland cement (OPC) [1]. Unlike other pozzolanic materials, BFS can be used as a hydraulic binder due to hydration characteristics that do not require the presence of lime. The hydraulic reactivity of these materials is further enhanced by alkaline solutions [2], which is ideal for the treatment of low activity nuclear waste located at the Savannah River Site and Hanford Site as these salt-based waste streams have pH values greater than 13.

We are interested in the properties of BFS as they relate to the retention of radionuclides in the salt waste streams [3-5]. The release of Cr, Tc, and NO_3^- can be significantly reduced by the addition of hydraulic blast furnace slag for Portland cement in the formulation of grout waste forms [3]. In this work, we hypothesize that these properties are due in some part to the glassy nature of the slag, and the dissolution/precipitation reactions that occur at the slag/solution interface. The process of glass corrosion has been studied for decades, and the fundamental mechanisms that drive the phenomena are understood [6-10] including mechanisms by which the original glass network transforms to secondary mineral phases during aqueous interactions. We postulate, that these same mechanisms that control the conversion from the glassy phase to secondary products in corroding glass systems must be similar to the mechanisms that control cementitious phase formation during hydration reactions involving the amorphous slag.

Understanding the fundamental interactions controlling the secondary product formation at the slag/solution interface is critical to designing concrete and grout formulations that optimize radionuclide retention and chemical durability. In addition, a foundational understanding of these properties would enable exploration of the design of synthetic, slag-like secondary cementitious materials with tighter compositional and structural tolerances.

The objective of this work is to initiate a study into the solution-mediated phase transformations that occur at the slag/solution interface for various solutions. We isolated certain, but not all, defining characteristics of a liquid salt waste stream and grout porewater, similar to that of the saltstone waste form at SRS, by creating various solutions for each characteristic (e.g., high pH, high salinity, calcium saturated, etc.) We conducted slag dissolution experiments in these various solutions to isolate the effects of each solution characteristic on the corrosion (hydration in cement science terminology) reactions at the slag/solution interface. By analyzing the leachate solution composition from each of these experiments, we can begin to understand how slag composition and solution chemistry are coupled in the formation of cementitious phases and other reaction products.

Variability in slag composition could affect the performance, overall durability, and the leachability of radionuclides from the grout waste form. In particular, variation of iron content could affect the reduction/oxidation reactions that govern the diffusivity of highly radioactive technetium species. A study in 2017 showed that while the secondary reaction products of chemically variable BFS were similar in nature, distinct difference existed in the short-range atomic ordering of the calcium-sodium aluminosilicate hydrate (C-(N)-A-S-H) phases. Given the desire to improve the retention of radionuclides by targeting specific secondary phases, these differences that may seem trivial from a construction standpoint, can prove detrimental in terms of nuclear waste form chemistry.

This interim report describes the initial results of experimental analyses conducted on a typical Salt Stone slag sample and provides a roadmap for: 1) finishing these initial analyses, 2) drawing conclusions from all the data collected, and 3) a work plan for continued development of a "designer slag" product that will replace the current use of BFS in low activity waste disposition – this synthetic slag would be produced by glass manufacturers and targeted specifically for low activity waste disposition via grouting.

2.0 Experimental Procedure

A blast furnace slag sample was obtained from a larger batch of material that was used to process waste at the Savannah River Site (SRS) in the second quarter of 2019. The BFS was procured from Lehigh Cement Company. A one-liter container of this BFS was subsampled using a spinning riffler into 8 smaller samples. The composition of the BFS was measured via X-ray fluorescence (XRF) spectroscopy and is given in Table 1. The sample-to-sample error in particle size distribution associated with spinning riffler samples is reportedly less than 1% [11]; accordingly, it was assumed that the distribution of particle sizes in all riffled subsamples was equal. This assumption is important as it allows us to consider the raw leachate concentrations when comparing samples, rather than normalizing to the sample surface area to volume ratio. An X-ray diffraction analysis of the BFS used in this work in shown in Figure 1 – the crystalline mineral phases are calcite and gypsum (which are sometimes added to BFS for enhanced reactivity[12-14]), and a large amorphous phase.

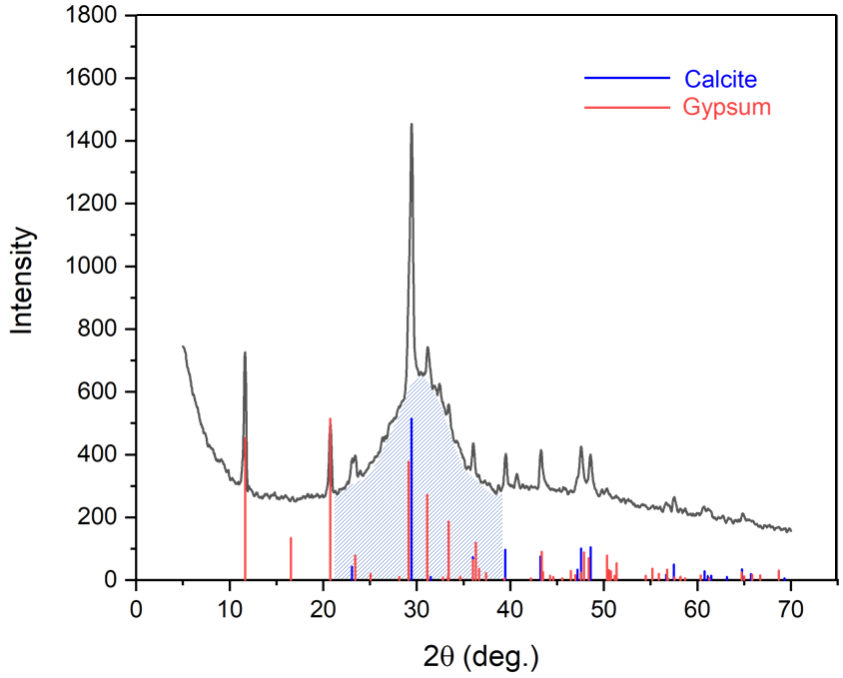

Figure 1: XRD showing the mineral phases present in the untreated BFS investigated in this work. The blue shaded region shows the large amorphous component of the slag. The crystalline phases intermixed with the amorphous slag are calcite and gypsum.

Table 1: Oxide composition of BFS used in the dissolution experiments (wt.%). "Ig" is loss on ignition.

CaO	SiO_2	Al_2O_3	Fe_2O_3	SO_3	MgO	K_2O	TiO_2	SrO	P_2O_5	Mn_2O_3	Ig	Sum
41.61	33.10	13.23	0.40	3.27	6.50	0.37	0.54	0.064	0.007	0.18	0.59	99.86

A total of 110 individual experiments were conducted involving BFS in contact with various solutions. The experimental matrix for these solutions in shown in Table 2. A "blank" experiment, i.e., a solution-only experiment, was also conducted for each of the solutions shown in Table 2. However, a separate experiment was not run for each individual blank duration, but rather the aliquots were subsampled from the blank vessel. Each duration in the solid BFS dissolution experiments was conducted in a separate digestion vessel. De-ionized (DI) water was used to prepare each solution.

Tank 50 Simulant – The Tank 50 simulant, shorthand "Tank 50", was prepared to mimic the composition of the liquid waste salt solution just prior to grout mixing at the Savannah River Site. The average blank composition of the simulant calculated by averaging each of the blank measurements for the various durations and the %RSD for these measurements is shown in Table 3.

Table 2: Experimental matrix of solutions and test durations. Replicate measurements of BFS dissolutions are indicated with a superscript "a" and replicate measurements of blank solutions are indicated with a superscript "b".

Solution	Starting pH	Durations (d)
DI H_2O	7	1[a],7,14,28,56
DI H_2O + 2 M NaCl	~7	1,7,14,28,56[a]
pH 12.5 NaOH	12.5	1[b],7[a,b],14[b],28[b],56[b]
pH 12.5 NaOH + 2 M NaCl	12.5	1,7,14,28[a],56
$Ca^{sat.}$ (calcium saturated)	12.5	1,7,14[a],28,56
$Ca^{sat.}$ + 2 M NaCl	12.6	1,7[a],14,28,56
2 M NaOH	>13	1,7,14,28[a],56
2 M NaOH + 2 M NaCl	>13	1[a],7[b],14[b],28[b],56[b]
Tank 50 Simulant	>13	1,7,14,28[a],56[a]

Table 3: Measured elemental concentrations in the Tank 50 simulant.

Element	Concentration (ppm)	Deviation (ppm)	%RSD
Al	5191.20	116.60	2.25
K	25.89	2.60	10.04
Na	129600.00	2302.20	1.78
S	2058.80	28.30	1.37
NO_3^-	1.83 M[*]	N/A	N/A
NO_2^-	0.62 M[*]	N/A	N/A
OH^-	2.3 M[†]	N/A	N/A

[*] Target compositions reported in molarity. Anions were not measured as part of the initial analyses.
[†] OH^- concentration was calculated using Geochemist's Workbench software (React).

2.1 Dissolution Experiments

The BFS dissolution experiments were conducted using the PCT-B method of ASTM C1285, "Determining Chemical Durability of Nuclear, Hazardous, and Mixed Waste Glasses and Multiphase Glass Ceramics: The Product Consistency Test (PCT)." The dissolutions were conducted in 23 ml, stainless steel Series 4700 General Purpose Pressure Vessel from Parr Instrument Company. The mass-to-volume ratio for the experiments was 1:10 – approximately 1.5 g of BFS was in contact with approximately 15 ml of solution for each duration shown in Table 2. The experiments were conducted at 50 °C. Upon completion of a given duration, the vessels were allowed to cool to room temperature prior to sampling or further analysis.

After cooling, the leachate solution (supernate) was decanted from the digestion vessel. A small aliquot of leachate was then acidified in preparation for chemical composition analysis via inductively-coupled plasma emission spectroscopy (ICP-ES). Another aliquot of the solution was retained for pH measurement (at room temperature). The vessels with the remaining solids were then placed into an oven at 50 °C to dry for solids analyses.

The acidified aliquots were measured via ICP-ES using an Agilent 5110 ES series spectrometer. Solution pH values were measured using a Fisher Scientific Accumet® AB150 pH Meter.

2.2 Solids Analyses

The dried BFS solids from each experiment have thus far been imaged using a Hitachi SU8200 Series Ultimate Cold Field Emission Scanning Electron Microscope (SEM). The dried samples were removed from the digestion vessels after removal from the drying oven, placed into glass sample vials, and stored in a desiccator prior to imaging. Small portions of the solids were removed from the vial and mounted with carbon tape on 30 mm SEM stubs prior to imaging – owing to the minimized charging associated with field emission SEM, no sample coating was needed to obtain the images presented in this report.

2.3 Quality Assurance

Requirements for performing reviews of technical reports and the extent of review are established in manual E7 2.60. SRNL documents the extent and type of review using the SRNL Technical Report Design Checklist contained in WSRC-IM-2002-00011, Rev. 2.

3.0 Results and Discussion

3.1 pH Measurements

The results of the pH measurements are shown in Figure 2. The recorded measurements are given in Table 4. Based on the results of these analyses, this particular slag composition has an apparent pH of approximately 11.5 in de-ionized water (DI H_2O) that is reached within 1 day of digestion at 50 °C. The DI H_2O + 2 M NaCl had a similar pH value to the DI H_2O only solution throughout the duration of the experiment. The neutral pH experiments are shaded green in Table 4.

Table 4: pH measurements recorded for each solution at the various experimental durations.

Time	DI H_2O	DI H_2O-2M NaCl	pH 12.5 NaOH	pH 12.5 NaOH+2M NaCl	Ca-sat.	Ca-sat. + 2M NaCl	2M NaOH	2M NaOH + 2M NaCl	Tank 50
1	11.7	11.5	12.2	11.9	12.3	11.9	13.4	13.4	13.6
7	11.5	11.6	12.2	11.8	12.2	11.8	13.1	13.0	13.3
14	11.6	11.6	12.2	11.8	12.2	11.8	13.1	13.0	13.3
28	11.6	11.7	12.3	11.9	12.3	11.9	13.1	13.0	13.2
56	11.7	11.8	12.3	11.9	12.3	11.9	13.1	12.9	13.2

The experiments that started at pH 12.5 (red shading in Table 4) decreased in pH, with the NaCl solution decreasing more than the salt-free solution. The Ca saturated experiments ($Ca^{sat.}$) (shaded blue in Table 4) demonstrated similar behavior to the pH 12.5 NaOH experiments in terms of pH value: the salt containing solution reached a lower pH value than the solution that did not contain salt. The 2M NaOH solutions (shaded orange in Table 4) had similar pH values throughout the experiment with the pH value of the NaCl containing solution being lower. However, at the high concentration of OH^- ions present in these solutions, this lower value is in fact, a greater difference in basicity than is present in the pH 12.5 solutions by a factor of 2-4 depending on the experimental duration. The measured pH of the Tank 50 experiment was consistent from days 7-56 at approximately 13.2-13.3 after dropping from the initial value of 13.6.

3.2 Solution Composition Analyses

The compositions of the various leachate solutions were measured via ICP-ES. Figure 3 shows the measured concentrations of the various leachate constituents for the various solutions by element. The concentrations in Figure 3 were corrected for the average background concentration of each solution taken from the average of the measured concentrations for each of the various solutions measured in the blank experiments. The concentrations in Figure 3 were not corrected for the dilution factor or normalized to the composition of the BFS.

The measured concentrations for the individual experiments, normalized to the mass fraction of the element in the BFS composition, along with an "average" uncertainty that was determined from replicate measurements, are shown in the following subsections. The mass fraction of an element in a composition is calculated by Equation 1.

$$f_i = x_o \frac{m_i}{M_o} \quad (1)$$

Where, f_i is the mass fraction of element "i" in the slag composition, x_o is the weight percent of the oxide containing element "i" in the composition, m_i is the molar mass of element "i", and M_o is the molar mass of the oxide containing element "i". The normalized concentration, corrected for the dilution factor of 20x, is then determined by dividing the corrected and normalized concentration by the mass fraction of the element being reported. This type of normalization is performed to evaluate the release of one element with respect to another element under a given set of conditions on a stoichiometric basis to investigate the congruency of the dissolution. The following subsections will discuss observations about the dissolution/leaching behavior of the BFS in the individual solutions – in addition to the solution data. Scanning electron microscopy images are presented for each solution of the solid specimens collected at 56 days to show the morphology of the samples. It is important to note here that any mineralogical identification based on the SEM images is purely speculative without X-ray diffraction analysis to confirm.

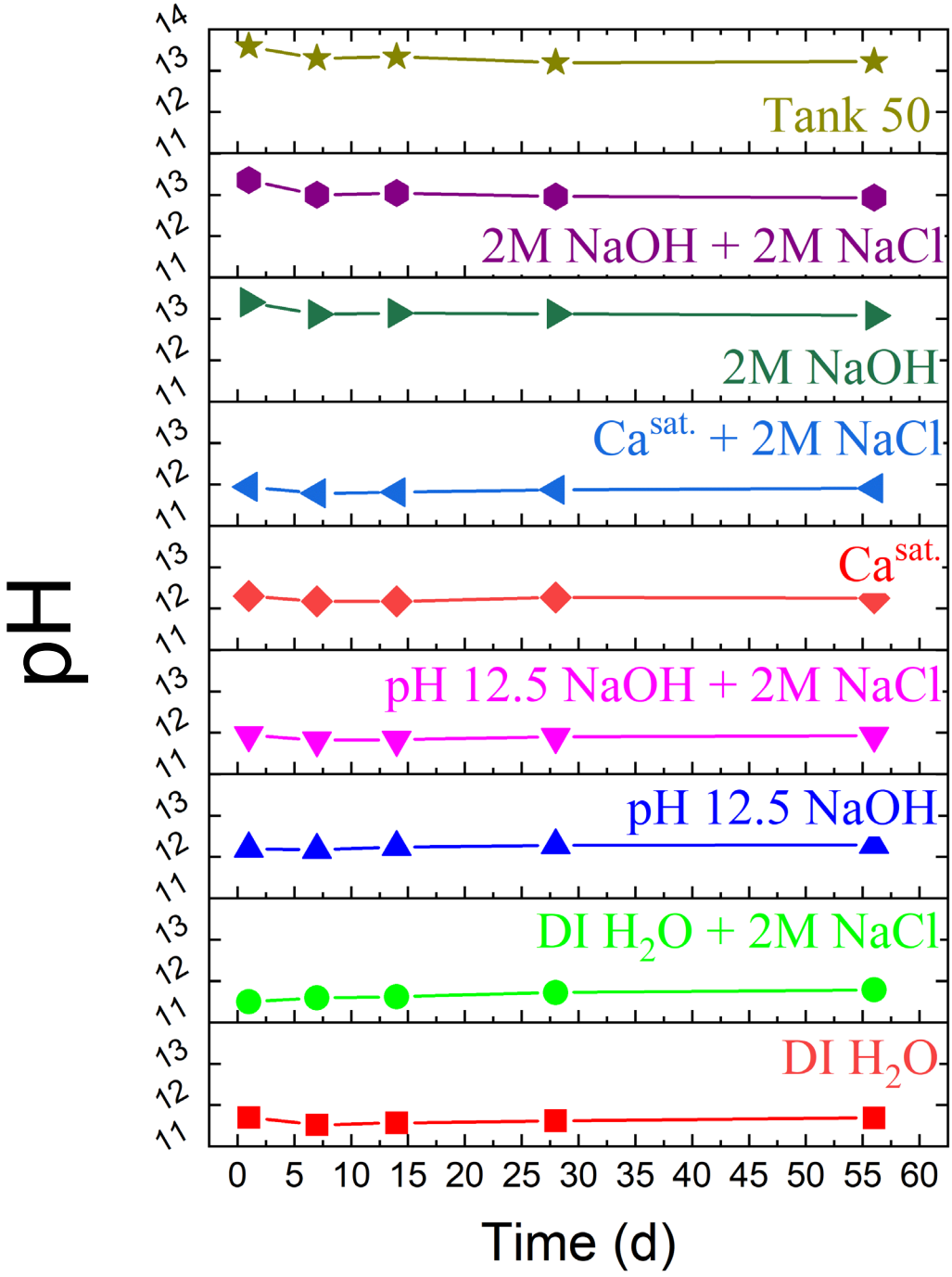

Figure 2: pH measurements of the BFS dissolution experiments.

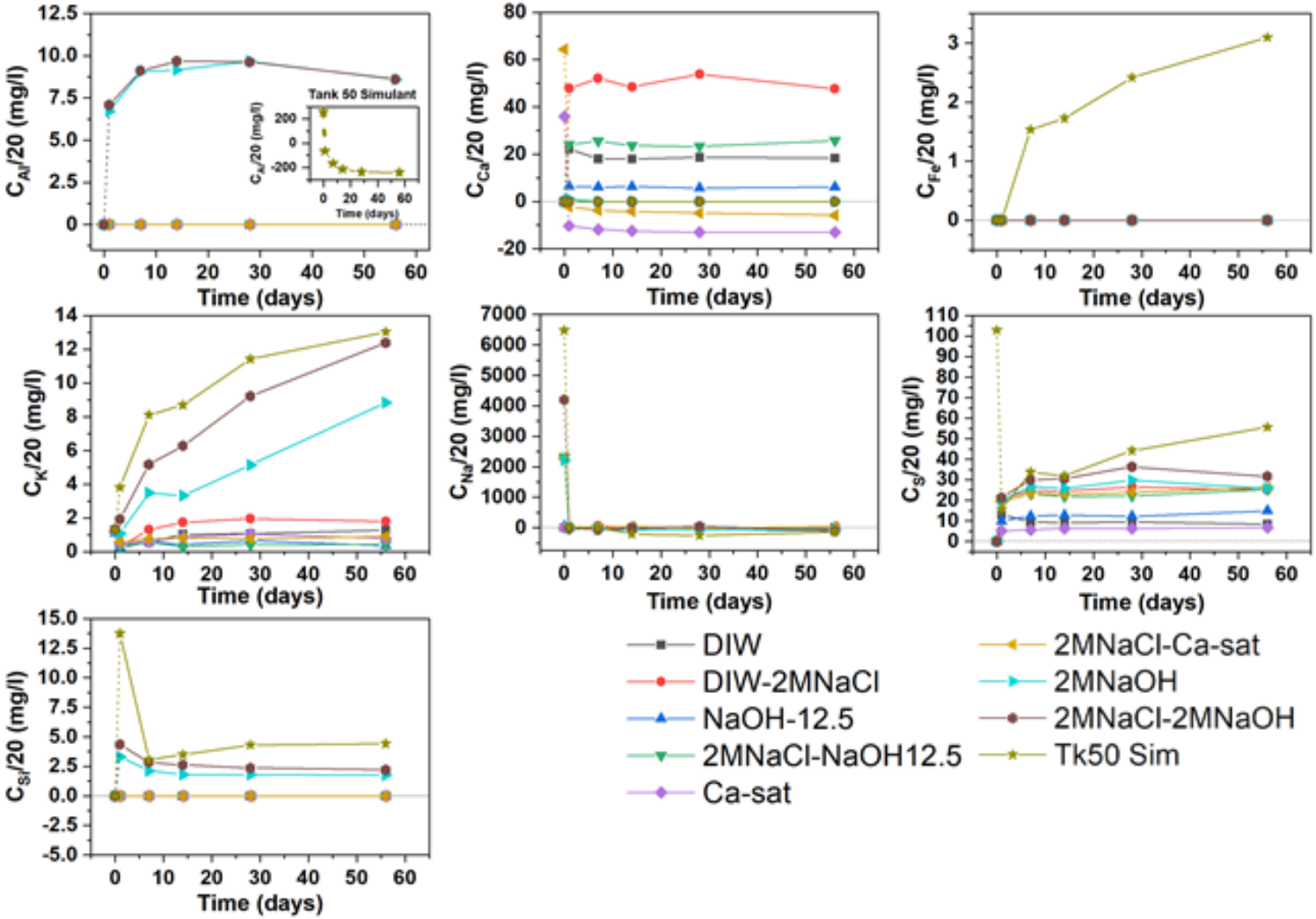

Figure 3: Measured concentrations of elements in leachate solutions from the various experiments. The dashed lines in each subplot represent the concentration difference between the average blank concentration and 1 day.

3.2.1 *De-Ionized Water (DI H_2O)*

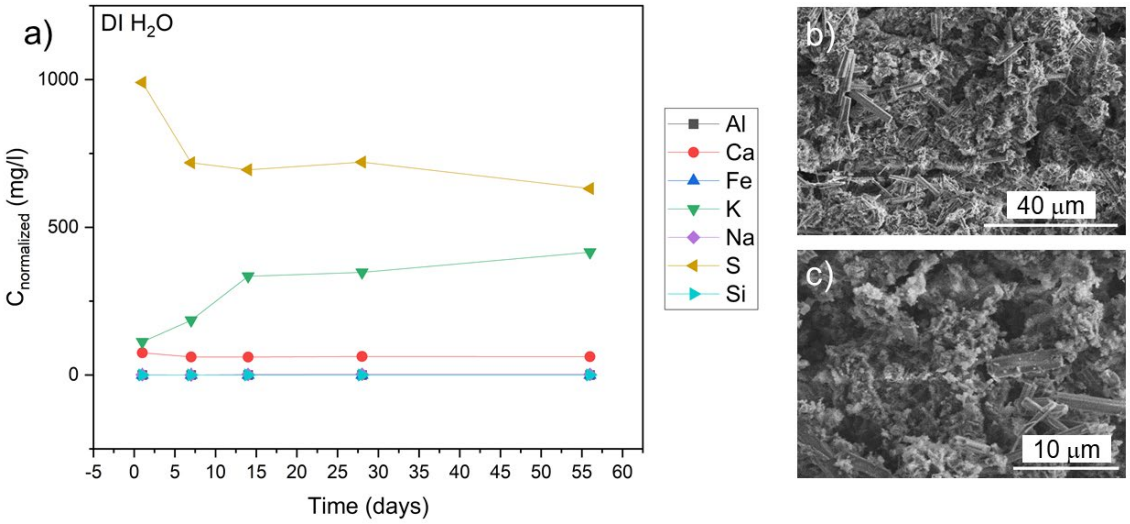

Figure 4: Normalized solution composition and SEM images of BFS in DI H_2O from 1 to 56 days. Note the possible ettringite formation visible in b) and c).

The measurements indicate that, relative to the other constituents in the slag, potassium and sulfur are highly soluble elements. Although potassium is highly soluble in this system, the concentration of K_2O in the BFS is less than 1% of the bulk solution composition and the release of this element is unlikely to contribute to the formation of significant mineral phases in the cementitious waste form. Sulfur, on the other hand, does play a factor in mineral phase formation, even in the DI H_2O experiment, as evidenced by the preliminarily identified ettringite formation observed via SEM in Figure 4b and 4c. The formation of this mineral phase may explain the observed decrease in the concentration of sulfur in Figure 4.

3.2.2 *DI H_2O + 2M NaCl*

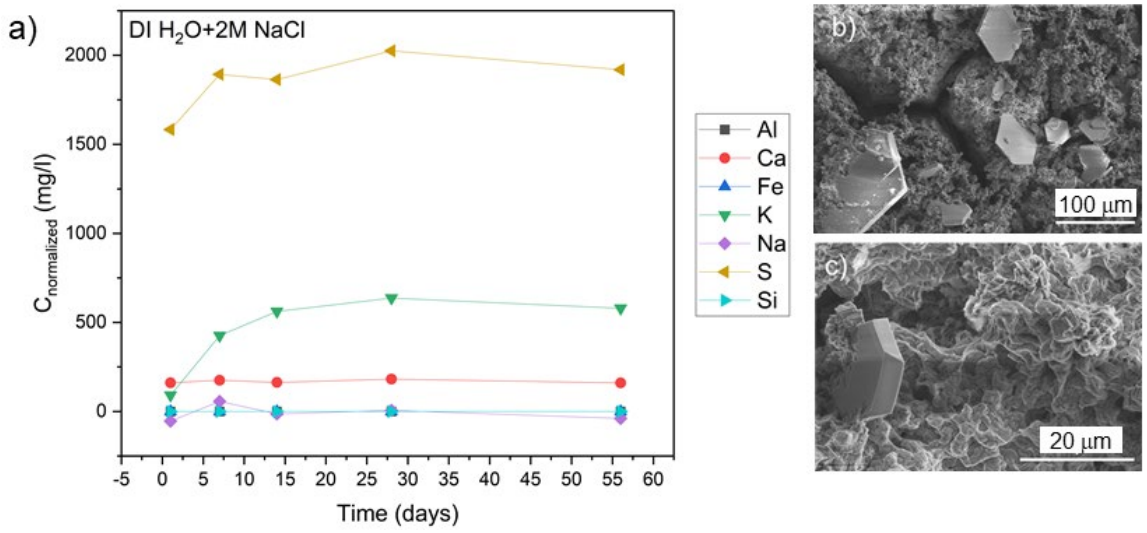

Figure 5: Normalized solution composition and SEM images of BFS in DI H_2O + 2 M NaCl from 1 to 56 days. The large hexagonal crystals seen in images b) and c) are likely Friedel's salts.

The ICP-ES measurements for the DI H_2O system that also contained 2 M NaCl again indicate the relative solubility of S compared to the other elements in the BFS composition. Also of note is the increased concentration of the Ca in the salt solution relative to the water-only, pH neutral solution. In fact, this experiment yielded the highest concentration of Ca measured in the solution any system at 56 days as shown in Figure 3. The SEM of these specimens revealed the formation of large, hexagonal crystals that are likely Ca-containing minerals like Friedel's salts (hydrocalumite). As with the DI H_2O experiment, there are other, poorly crystalline in appearance, phases present in the SEM images. The mineral identification of these phases requires additional analysis such as X-ray diffraction. It should be noted that nothing appearing like ettringite was observed forming in this system. Correspondingly, no drop in the S concentration was measured in this system over the duration, which was hypothesized to be related to ettringite formation in the DI H_2O system.

3.2.3 *pH 12.5 (NaOH)*

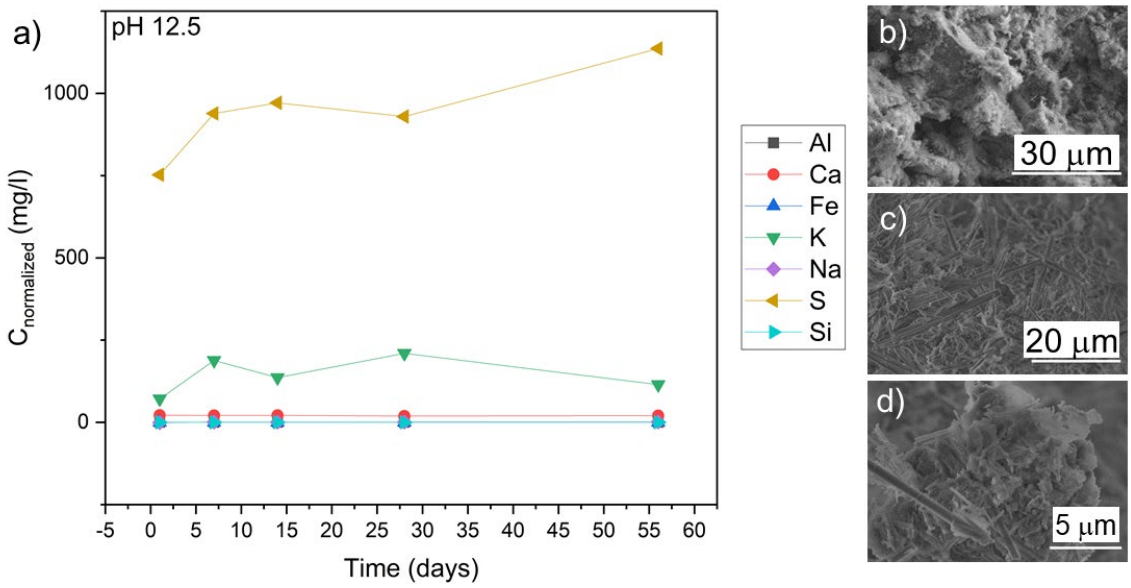

Figure 6: Normalized solution composition and SEM images of BFS in pH 12.5 (NaOH adjusted) solution from 1 to 56 days. The SEM images reveal what appear to be calcium silicate hydrate (CSH)-related phases (b) and ettringite (c,d – needle like structures).

Again, S and K are the most soluble elements in the pH 12.5 system relative to the elemental concentration in the glasses. The normalized concentration of these elements in the pH 12.5 system is lower than in the near-neutral pH experiment, DI H_2O + 2M NaCl, but higher than in the DI H_2O solution. No Al and very little Ca was observed in the pH 12.5 system, which is likely an indication of the pozzolanic reactivity of the BFS samples. The SEM image Figure 6b shows what appears to be CSH-like phases. The images in Figure 6c and 6d appear to show similar poorly crystalline phases interspersed with crystals that were tentatively identified as ettringite.

3.2.4 *pH 12.5 (NaOH) + 2M NaCl*

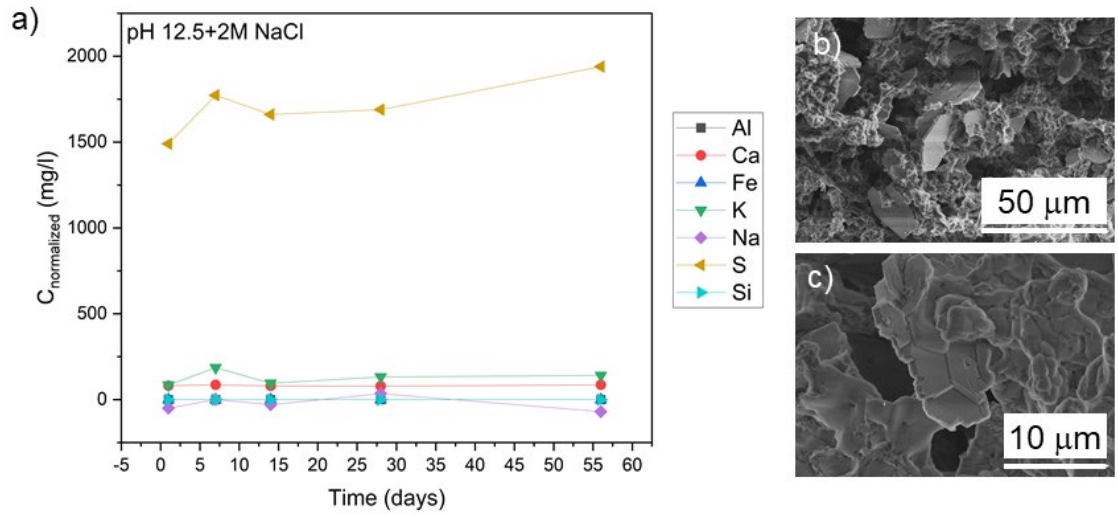

Figure 7: Normalized solution composition and SEM images of BFS in pH 12.5 (NaOH adjusted) with 2M NaCl in solution from 1 to 56 days. The SEM images, Figure 7b and 7c, show what appear to be CSH-like phases as well as Friedel's salts. The hexagonal crystals in Figure 7c may also be stratlingite.

The pH 12.5 + 2M NaCl system demonstrated similar behavior to the DI H_2O + 2M NaCl system in that the presence of the salt increases the solubility of both Ca and S. The amount of S measured in the system is approximately equal to the amount measured in the DI H_2O + 2M NaCl experiment; however, the amount of Ca measured in both the pH 12.5 and pH 12.5 + 2M NaCl experiments was only half the amount measured in the water experiments. This is likely due to enhanced mineralization in the higher pH systems. The appearance of Friedel's salt-like phases and potentially stratlingite in the pH 12.5 + 2M NaCl are consistent with reported behavior of slag in briny solutions [15].

3.2.5 *Calcium Saturated ($Ca^{sat.}$)*

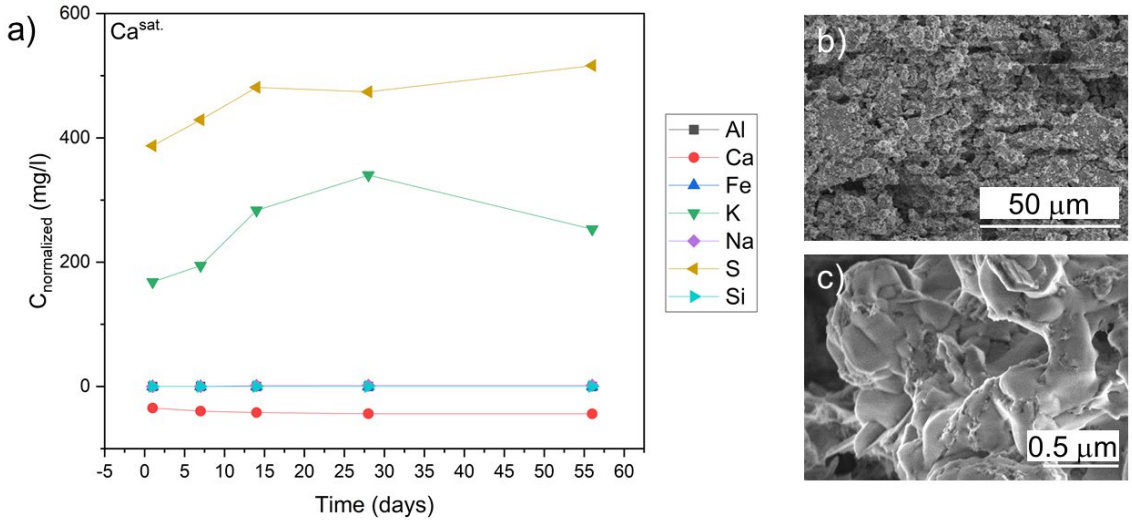

Figure 8: Normalized solution composition and SEM images of BFS in $Ca^{sat.}$ solution from 1 to 56 days. The SEM images in Figures 8b and 8c show what is likely calcium hydroxide phases formed during the hydration of the slag in the $Ca^{sat.}$ solution.

The normalized concentration of S in the $Ca^{sat.}$ system was the lowest of any of the experiments conducted. Similarly, the normalized concentration of K was lower than measured in the DI H_2O (with and without NaCl) experiments but higher than what was measured in the pH 12.5 (with and without NaCl) experiments. This lowered K concentration could be caused by several mechanisms that are not necessarily exclusive: 1) the Ca concentration in the solution suppresses the dissolution of the BFS, 2) K is being consumed in the pozzolanic reactions that form the binding CSH-based phases (e.g., C-(Na,K)-S-H), and/or 3) the rapid reaction on the BFS surface to form CSH phases creates an altered layer that inhibits diffusion (via ion exchange) of K from the BFS matrix. The background corrected concentration of Ca in this experiment was less than zero, which indicates consumption via pozzolanic reaction of some of the initially present Ca. Approximately, 29% of the original Ca in the system was fixed by the BFS within the first 24 hours and approximately 36% was fixed at 56 days indicating the most of the pozzolanic reaction occurs very early on in the BFS hydration.

3.2.6 *Ca$^{sat.}$ + 2M NaCl*

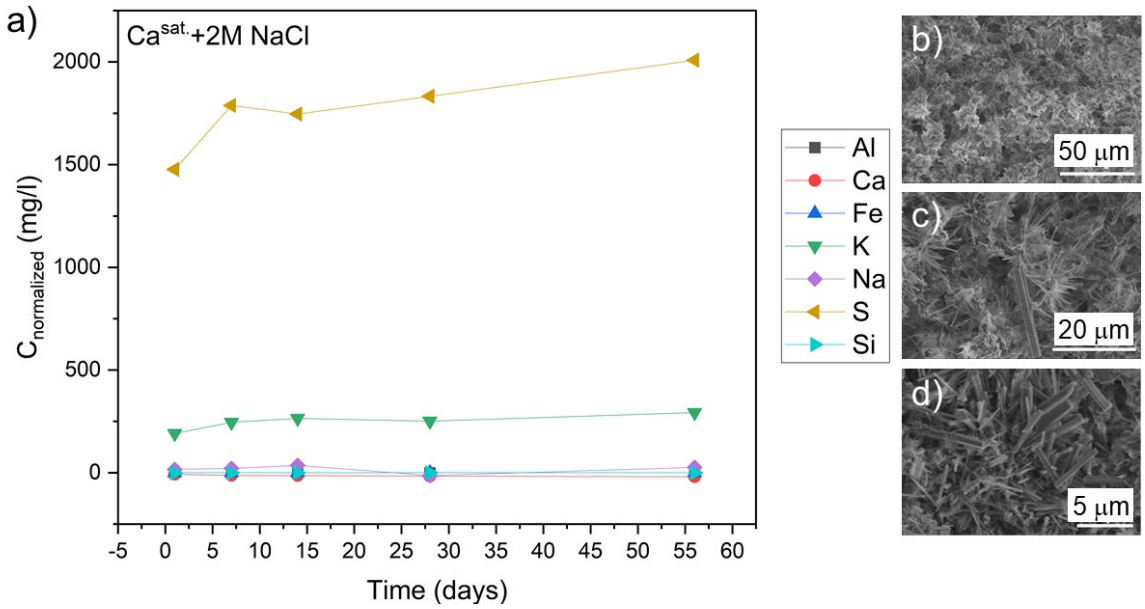

Figure 9: Normalized solution composition and SEM images of BFS in Ca$^{sat.}$ + 2M NaCl solution from 1 to 56 days. The SEM images in Figures 9b, 9c, and 9d show a high degree of potential ettringite formation as well as what appears to be CSH-like phases.

The measured concentration of S in the Ca$^{sat.}$ + 2M NaCl experiment is one of the highest observed for any of the experiments in this work. In addition to the high solution concentration of S, prolific ettringite formations were observed via SEM as shown in Figure 9b, 9c, and 9d. The measured concentration of Ca in the Ca$^{sat.}$ + 2M NaCl system was not as low as was measured in the Ca$^{sat.}$ experiment without the NaCl addition. Interestingly, it is well known that the solubility limit of Ca in water increases with increasing Cl^- concentration; however, the observation of higher Ca in the Ca$^{sat.}$ + 2M NaCl relative to the Ca$^{sat.}$ experiment poses an interesting question: Is the higher value of Ca in the salt-based solution caused by the higher solubility of Ca in this system, or is the high salt concentration suppressing the pozzolanic reactions occurring at the slag/solution interface? In terms of the amount of Ca fixed from the initial solution throughout the course of the experiment, the value is significantly lower for the NaCl-containing solution relative to what was observed in the Ca$^{sat.}$ solution (approximately 36% in Ca$^{sat.}$ at 56 days compared to approximately 9% in Ca$^{sat.}$ + 2M NaCl at 56 days). So, it would seem that at this cursory level, this observation is evidence that Cl^- suppresses the pozzolanicity of BFS.

3.2.7 *2M NaOH*

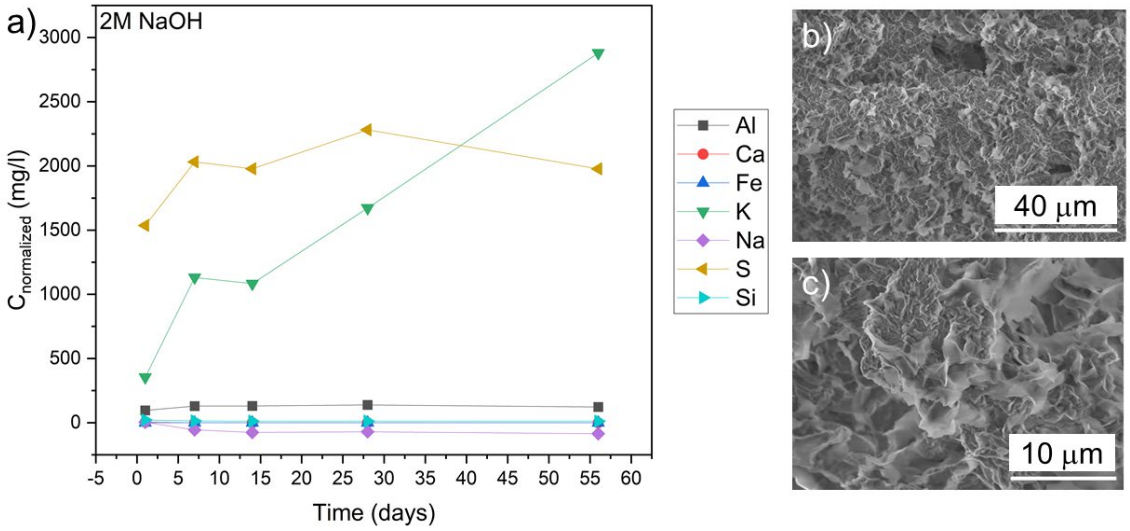

Figure 10: Normalized solution composition and SEM images of BFS in 2M NaOH solution from 1 to 56 days. The SEM images in Figure 10b and 10c show what appear to be CSH phases that are present in other experiments but an additional phase that may be a tobermorite mineral phase.

The 2M NaOH experiment was one of three experiments to register a detectable amount of Al in the leachate solution. The presence of Al is likely indicative of an aggressive dissolution of the BFS matrix relative to the hitherto reported solutions. Similar to the appearance of Al, this experiment was also one of only three experiments to record a detectable level of Si in solution, which is more evidence of aggressive dissolution of the BFS matrix. No Ca was detectable in the solution beyond 1 day, which is not surprising given the solubility of Ca with respect to the high pH of the solution. What is indicated by all of these observations is that the BFS was dissolving in the solution to such a degree that the Al and Si being released could not be completely sequestered in phases that also contain Ca, such as CSH. The massive release of K (keeping in mind this is normalized to the amount of K in the original BFS composition) is also suggestive of aggressive dissolution relative to the other samples. The S content in the 2M NaOH experiment is consistent with concentrations observed in the $Ca^{sat.}$ + NaCl, pH 12.5 + NaCl, and DI H_2O + NaCl at 56 days and slightly lower than the 2M NaOH + 2M NaCl (not yet discussed) at 56 days. The concentration is higher than all previously mentioned experiments not included in the list above. A noteworthy observation is the "settling" of S concentrations on approximately the same value in the following experiments: $Ca^{sat.}$ + NaCl, pH 12.5 + NaCl, and DI H_2O + NaCl, and 2M NaOH. This behavior could be anomalistic or indicative of some underlying transient mechanism involving S that is playing out on a longer time scale than most of the previously discussed mechanisms.

3.2.8 *2M NaOH + 2M NaCl*

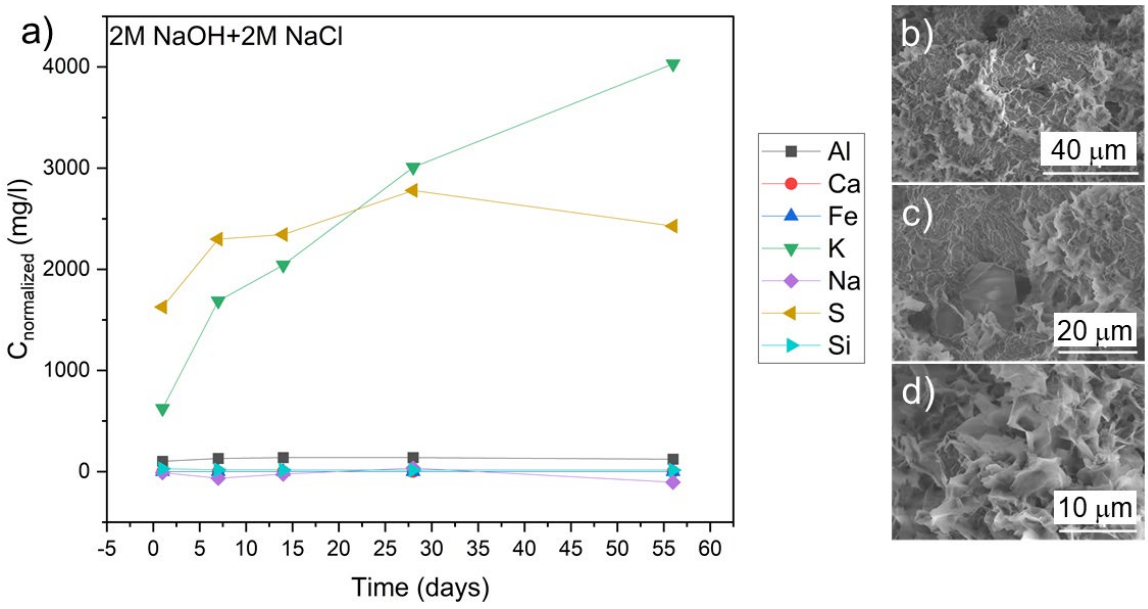

Figure 11: Normalized solution composition and SEM images of BFS in 2M NaOH + 2M NaCl solution from 1 to 56 days. The SEM images in Figures 11b, 11c, and 11d show a similar phase to what was observed in the 2M NaOH, i.e., potentially tobermorite. The nearly prismoidal crystal in Figure 10c is potentially katoite, which is a Si-free hydrogarnet.

The 2M NaOH + 2M NaCl experiment recorded the highest 1-day concentration of S for any of the experiments conducted. This experiment also had detectable levels of Al and Si, which, similar to the 2M NaOH system, is indicative of a more aggressive BFS matrix dissolution than what occurred with the previously discussed initial solution compositions. The Al concentration in the 2M NaOH + 2M NaCl experiment was approximately equal to what was measured in the 2M NaOH without salt solution and the amount of Si in the salt bearing solution was slightly higher than in the non-salt containing 2M NaOH solution. Again, zero calcium was detected in the system, which is consistent with what was observed in the 2M NaOH system – this lack of calcium combined with the measurable concentrations of Si and Al signaling matrix dissolution into the leachate implies that all of the Ca "released" from the slag is being consumed in secondary phases.

3.2.9 *Simulated Tank 50 (SRS) Solution*

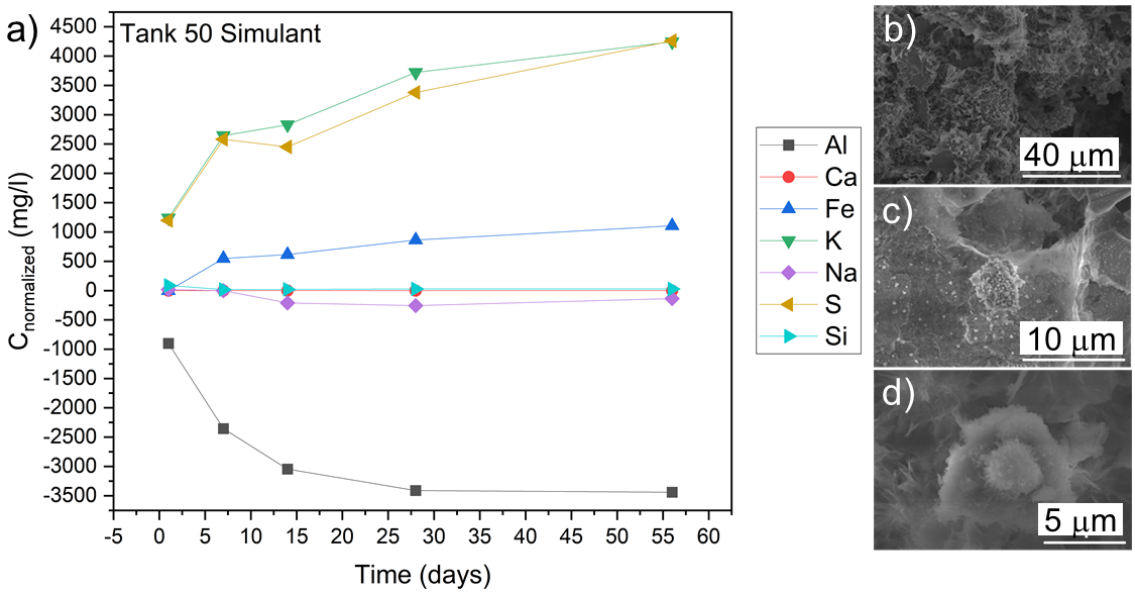

Figure 12: Normalized solution composition and SEM images of BFS in Tank 50 simulant solution from 1 to 56 days. The SEM images in Figure 12b, 12c, and 12d show similar CSH-like phases relative to those observed in the other systems, but also an example of a unique crystalline phase to the Tank 50 experiment.

The initial composition of the Tank 50 simulant solution was quite different from any of the other solution-systems tested in this work as demonstrated by the data presented in Table 3. A significant portion of the initial Al present in the solution was consumed throughout the duration of the experiment. In addition, Na was also consumed as evidenced by the negative corrected and normalized concentration. This is likely due to the precipitation of secondary mineral phases, perhaps zeolites (see Figure 12c and 12d). However, XRD would be necessary to determine what specific phases were consuming the Al. Interestingly, the Tank 50 simulant experiment was the only system to have a measurable concentration of Fe in the leachate solution. This is notable because of the low concentration of Fe in the slag composition (0.4 wt%) and that no Fe was measured in the Tank 50 simulant blank experiments. This presence of Fe in the leachate is suggestive of aggressive BFS matrix dissolution. Similar to the 2M NaOH solution with and without NaCl, no Ca was measured in the Tank 50 experiment for the entirety of the experiment. The K and S normalized concentrations were approximately equal throughout the duration of this experiment.

4.0 Conclusions

Nine different solutions were examined during this work. Not surprisingly, the rate of apparent matrix dissolution appears to be strongly correlated with the initial pH of the leachate solution. For instance, the only system in which Fe was measured in the leachate solution also had the highest starting pH – this is similar behavior to that which occurs in corroding glass systems. Many potential mineral phases were speculatively identified via visual observation of SEM images including: ettringite, CSH, Friedel's salts, stratlingite, tobermorites, and zeolites. Leachate solution composition measurements indicated that of the base slag composition, K and S are the most soluble elements and appear in all solutions in high relative concentrations even after only one day of leaching – the high sulfur concentrations likely resulted from the added gypsum. The most

notable conclusion that can be drawn from this initial work is that the presence of chlorine in the initial leachate solution has a significant effect on both the dissolution rate and/or solubility of certain elements as well as the mineral phases formed throughout the experiments. For example, the presence of Cl in solution significantly affects the solubility of Ca in solutions with initial pH of 12.5 or less (it should be noted that this enhanced solubility in the presence of Cl was not observed in the 2M NaOH systems). The solutions that contained NaCl also had higher concentrations of S present.

5.0 Recommendations, Path Forward or Future Work

In order to fully understand the effects of the different initial solution compositions on the dissolution/precipitation reactions occurring in BFS samples, the solids must be analyzed via XRD to understand the mineral evolution throughout the course of the experiments. This will provide further insight into the dissolution characteristics of the initial mineral phases present in the BFS versus the glassy component. Given what is known about the mineralogy of the slag studied in this work (see Figure 1), it is likely that the beneficial properties that BFS imparts on low activity waste grout formulations arise as a result of the dissolution or transformation of the glassy phase. Subsequently, any designer material meant to replace BFS would need to be based primarily on the chemical and physical properties of the amorphous phase.

6.0 References

1. Bertonlini, L., et al., *Corrosion of Steel in Concrete*. 2004, KGaA, Weinheim: Wiley-VCH Verlag GmbH & Co.
2. Raafat, I., et al., *Slag Cement-Low Level Radioactive Waste Forms at Savannah River Plant.* American Ceramic Society Bulletin, 1986. **65**(12): p. 1578-1583.
3. Langton, C.A., *Slag-Based Saltstone Formulations.* MRS Proceedings, 1988. **112**: p. 61-70.
4. Westsik, J.H., et al., *Supplemental Immobilization of Hanford Low-Activity Waste: Cast Stone Screening Tests*, 2013, Pacific Northwest National Laboratory (PNNL), Richland, WA (US),
5. Harbour, J., et al., *Characterization of slag, fly ash and portland cement for saltstone*, 2006, Citeseer,
6. Sanders, D.M. and L.L. Hench, *Mechanisms of Glass Corrosion.* Journal of the American Ceramic Society, 1973. **56**(7): p. 373-377.
7. Grambow, B. and R. Müller, *Chemistry of Glass Corrosion in High Saline Brines.* MRS Proceedings, 2011. **176**: p. 229.
8. Grambow, B., *A general rate equation for nuclear waste glass corrosion.* MRS Online Proceedings Library Archive, 1984. **44**.
9. Bunker, B.C., *Molecular mechanisms for corrosion of silica and silicate glasses.* Journal of Non-Crystalline Solids, 1994. **179**(Supplement C): p. 300-308.
10. Clark, D.E., C.G. Pantano, and L.L. Hench, *Corrosion of Glass*. 1979, New York, NY: Books for Industry and the Glass Industry.
11. Jillavenkatesa, A., S.J. Dapkunas, and L.-S.H. Lum, *Particle size characterization*. Vol. 960. 2001: National Institute of Standards and Technology Washington, DC.
12. Magallanes-Rivera, R.X. and J.I. Escalante-García, *Anhydrite/hemihydrate-blast furnace slag cementitious composites: Strength development and reactivity.* Construction and Building Materials, 2014. **65**: p. 20-28.
13. Mun, K.J., S.Y. So, and Y.S. Soh, *The effect of slaked lime, anhydrous gypsum and limestone powder on properties of blast furnace slag cement mortar and concrete.* Construction and Building Materials, 2007. **21**(7): p. 1576-1582.
14. Park, H., et al., *Strength enhancement and pore-size refinement in clinker-free CaO-activated GGBFS systems through substitution with gypsum.* Cement and Concrete Composites, 2016. **68**: p. 57-65.
15. Shao, Y., et al., *Identification of chromate binding mechanisms in Friedel's salt.* Construction and Building Materials, 2013. **48**: p. 942-947.

Distribution:

S. L. Marra, 773-A
T. B. Brown, 773-A
D. R. Click, 999-W
S. D. Fink, 773-A
C. C. Herman, 773-A
E. N. Hoffman, 999-W
F. M. Pennebaker, 773-42A
M. E. Stone, 999-W
A.D. Cozzi, 999-W
B. Garcia-Diaz, 999-2W
J. Manna, 999-W
Records Administration (EDWS)